Walden-Inversion-Enforced Transition-State Stabilization in a Protein Tyrosine Phosphatase

Cristobal Alhambra,[†] Li Wu,[‡] Zhong-Yin Zhang,*[,‡] and Jiali Gao*[,†]

Contribution from the Department of Chemistry, State University of New York at Buffalo, Buffalo, New York 14260, and Department of Molecular Pharmacology, Albert Einstein College of Medicine, Bronx, New York 10461

Received July 29, 1997

Abstract: The initial step of the dephosphorylation reaction of a tyrosine phosphate substrate catalyzed by the low molecular weight bovine protein tyrosine phosphatase (BPTP) has been studied, making use of a combined quantum mechanical and molecular mechanical approach in molecular dynamics simulations. It was found that the enzyme favors a dianion substrate in the dephosphorylation reaction, which is consistent with experiments but in contrast to a recent mechanistic proposal involving a monoanion phosphate. The computed activation free energy is ca. 14 kcal/mol, in accord with the activation parameters determined in the present study from stopped-flow kinetics experiments. Structural analyses support the finding that BPTP catalyzes dephosphorylation reactions by stabilizing the transition state through Walden-inversion-enforced hydrogen-bonding interactions during the S_N2 process.

Protein phosphorylation and dephosphorylation are fundamental processes in cellular signal transduction pathways, which mediate cell growth, proliferation, and differentiation.[1] The reversible phosphorylation is catalyzed by groups of enzymes known as protein kinases and phosphatases. Specific protein tyrosine phosphatases (PTPases) are involved in a variety of cellular responses and regulatory mechanisms.[2] PTPases can be grouped into two classes, including the receptor-like and intracellular protein tyrosine phosphatases.[3] The receptor-like PTPases generally have an extracellular domain, a transmembrane region, and two cytoplasmic PTPase domains. The intracellular PTPases contain a single catalytic domain and various terminal extensions including the Src homology 2 (SH2) domain. Although PTPases are diverse in size and structural organization, their catalytic segments usually span about 250 residues. In addition, a distinct class of cytoplasmic low molecular weight (M_r) PTPases (18 kD) has been found in mammals, yeast, and bacteria.[4] Although there is little sequence homology between the high and low molecular weight enzymes, the hallmark of these PTPases is the universal sequence of $C(X)_5R$-(S/T) at the active site, giving rise to the notion of PTPase signature motif.[3]

A number of crystal structures of protein tyrosine phosphatases have been determined, including the bovine PTPase (BPTP),[5] the catalytic domain of human PTP1B,[6] and the *Yersinia* PTPase.[7] Structural and biochemical studies demonstrate that these enzymes share a common mechanism of catalysis with the initial formation of a phosphate thioester intermediate, which is subsequently hydrolyzed by water.[3,8,9] Each of the two steps involves a Walden inversion of configuration at the phosphorus center in the $S_N2(P)$ process. The invariant Cys residue (e.g., Cys12 in BPTP, Cys215 in PTP1B, and Cys403 in the *Yersinia* PTPase) has been identified as the nucleophile in the initial step, and the invariant Arg at the end of the catalytic loop is necessary for both substrate binding and transition-state stabilization.[5−7] Because of the biological importance of phosphate hydrolysis, there have been numerous experimental investigations, and there is continuous interest in the understanding of the detailed catalytic mechanism for dephosphorylation reactions.[2−10] Early computational studies of phosphate hydrolysis are exemplified by gas-phase geometry

[†] State University of New York at Buffalo.

[‡] Albert Einstein College of Medicine.

(1) (a) Fischer, E. H.; Charbonneau, H.; Tonks, N. K. *Science* **1991**, *253*, 401. (b) Charbonneau, H.; Tonks, N. K. *Annu. Rev. Cell Biol.* **1992**, *8*, 463. (c) Walton, K.; Dixon, J. E. *Annu. Rev. Biochem.* **1993**, *62*, 101.

(2) (a) Shultz, L. D.; Schweitzer, P. A.; Rajan, T. V.; Yi, T.; Ihle, J. N.; Matthews, R. J.; Thomas, M. L.; Beier, D. R. *Cell* **1993**, *73*, 1445. (b) Pingel, J. T.; Thomas, M. L. *Cell* **1989**, *58*, 1055. (c) Perkins, L. A.; Larsen, I.; Perrimon, N. *Cell* **1992**, *70*, 225. (d) Guan, K. L.; Dixon, J. E. *Science* **1990**, *249*, 553.

(3) For recent reviews, see: (a) Zhang, Z.-Y. *Curr. Top. Cellular Regul.* **1997**, *35*, 21. (b) Fauman, E. B.; Saper, M. A. *Trends Biochem. Sci.* **1996**, *21*, 413.

(4) (a) Waheed, A.; Laider, P. M.; Wo, Y.-Y. P.; Van Etten, R. L. *Biochemistry* **1988**, *27*, 4265. (b) Zhang, Z.-Y.; Van Etten, R. L. *Arch. Biochem. Biophys.* **1990**, *228*, 39. (c) Camici, G.; Manao, G.; Cappugi, G.; Modesti, A.; Stefani, M.; Ramponi, G. *J. Biol. Chem.* **1989**, *264*, 2560.

(5) (a) Stuckey, J. A.; Schubert, H. L.; Fauman, E. B.; Zhang, Z.-Y.; Dixon, J. E.; Saper, M. A. *Nature* **1994**, *370*, 571. (c) Fauman, E. B.; Yuvaniyama, C.; Schubert, H. L.; Stuckey, J. A.; Saper, M. A. *J. Biol. Chem.* **1996**, *271*, 18780.

(6) (a) Zhang, M.; Van Etten, R. L.; Stauffacher, C. V. *Biochemistry* **1994**, *33*, 11097. (b) Su, X.-D.; Taddei, N.; Stefani, M.; Ramponi, G.; Nordlund, P. *Nature* **1994**, *370*, 575. (c) Logan, T.; Zhou, M.-M.; Nettesheim, D. G.; Meadows, R. P.; Van Etten, R. L.; Fesik, S. W. *Biochemistry* **1994**, *33*, 11087. (d) Zhang, M.; Zhou, M.; Van Ettern, R. L.; Stauffacher, C. V. *Biochemistry* **1997**, *36*, 15.

(7) (a) Barford, D.; Flint, A. J.; Tonks, N. K. *Science* **1994**, *263*, 1397. (b) Barford, D.; Jia, Z.; Tonks, N. K. *Nat. Struct. Biol.* **1995**, *2*, 1043. (c) Jia, Z.; Barford, D.; Flint, A. J.; Tonks, N. K. *Science* **1995**, *268*, 1754.

(8) (a) Zhang, Z.-Y.; Van Etten, R. L. *J. Biol. Chem.* **1991**, *266*, 1516. (b) Zhang, Z.-Y.; Van Etten, R. L. *Biochemistry* **1991**, *30*, 8954. (c) Zhang, Z.-Y.; Davis, J. P.; Van Etten, R. L. *Biochemistry* **1992**, *31*, 1701. (d) Saini, M. S.; Buchwald, S. C.; Van Etten, R. L.; Knowles, J. R. *J. Biol. Chem.* **1981**, *256*, 10453. (e) Davis, J. P.; Zhou, M.-M.; Van Etten, R. L. *Biochemistry* **1994**, *33*, 1278.

(9) (a) Guan, K. L.; Dixon, J. E. *J. Biol. Chem.* **1991**, *266*, 17026. (b) Cho, H.; Krishnaraj, R.; Kitas, E.; Bannwarth, W.; Walsh, C. T.; Anderson, K. S. *J. Am. Chem. Soc.* **1992**, *114*, 7296.

(10) (a) Westheimer, F. H. *Science* **1987**, *235*, 1173. (b) Westheimer, F. H. *Chem. Rev.* **1981**, *81*, 313. (c) Thatcher, G. R. J.; Kluger, R. *Adv. Phys. Org. Chem.* **1989**, *25*, 99. (d) Admiraal, S. J.; Hershlag, D. *Chem. Biol.* **1995**, *2*, 729.

S0002-7863(97)02578-X CCC: $15.00
Published on Web 04/11/1998

optimizations using ab initio methods.[11] Recently, Warshel and co-workers, using the empirical valence bond approach, carried out a series of simulations aimed at understanding phosphate hydrolysis in enzymes.[12] These studies constitute the basis for further investigations of this important reaction. The formation of a phosphocysteine intermediate in the PTPase-catalyzed reactions is particularly interesting,[8,13] since thiophosphate linkage in proteins has only been observed in bacterial thioredoxin and mannitol carrier-specific transport enzyme II.[3] Although thiophosphate linkage has been suggested as an intermediate in enzymatic phosphorylation reactions,[14] its biological importance has only recently begun to be appreciated.[3,8,9,13] Consequently, computational investigations of the reaction mechanism employing hybrid quantum mechanical and classical potentials are warranted to gain an understanding of phosphate thioester as an intermediate in phosphoryl transfer processes.

In this paper, we report a computational study of the initial step of the enzymatic process in a prototypical low M_r PTPase, the bovine PTPase (BPTP).[5] The computational results support that PTPases catalyze dephosphorylation reactions by stabilizing the transition state through Walden-inversion-enforced hydrogen-bonding interactions in the active site. In addition, free energy profiles for the reactions of phosphotyrosine monoanion and dianion were determined in BPTP. We found that there is no special energetic advantage for the reaction between Cys12 thiolate and tyrosine phosphate monoanion in the active site, in contrast to the recent proposal that the phosphate monoanion is the substrate in BPTP.[15] In the following, computational details are first given, followed by results and discussion.

Computational and Experimental Details

A. Hybrid Quantum Mechanical and Molecular Mechanical Potential. Determination of reaction surfaces in protein is necessary for the refinement of mechanistic ideas on enzyme catalysis. On the theoretical side, significant progress has been made in our laboratory and others with the development of hybrid quantum mechanical and molecular mechanical (QM/MM) methods for the study of chemical reactions in solution.[16−18] In this approach, the substrate and other critical residues in the active site are treated explicitly by a quantum chemical method, whereas the rest of the protein and solvent molecules are represented by molecular mechanics force fields. Thus, the effective Hamiltonian of the system is given by eq 1

$$\hat{H}_{\text{eff}} = \hat{H}_{\text{qm}} + \hat{H}_{\text{qm/mm}} + \hat{H}_{\text{mm}} \quad (1)$$

where H_{qm} is the Hamiltonian for the quantum mechanically treated active site, $H_{\text{qm/mm}}$ describes the electrostatic and van der Waals interactions between the QM and MM region, and H_{mm} is the molecular mechanics energy for the classical protein−solvent system. Since electronic structure calculations are explicitly carried out in the computer simulation, the method may be used to study chemical reactions in the enzyme active site. We have employed this approach to investigate a variety of chemical processes in aqueous and organic solutions, making use of both semiempirical and ab initio quantum mechanical methods.[16,19] Encouraging results have been obtained, demonstrating the reliability of hybrid QM/MM potentials in condensed-phase simulations. Since details of the hybrid QM/MM method have been described in several recent articles, they will not be repeated here. Interested readers are directed to refs 16 and 17.

It is, of course, desirable to use ab initio molecular orbital or density functional theory in the hybrid QM/MM approach;[19f] however, such computations are still too time-consuming to be practical for applications involving the determination of free energy profiles for enzyme-catalyzed reactions using molecular dynamics simulation methods. In the present study, we have adopted the semiempirical AM1 and MNDO methods developed by Dewar and co-workers to describe the active site region.[20] Figure 1 depicts the "quantum mechanical" residues that are directly involved in the thiophosphate ester formation. These include the nucleophilic residue Cys12, the substrate tyrosine phosphate, and the Brønsted acid catalytic residue Asp129. The CHARMM-22 force field is used to represent all other protein atoms along with the three-site TIP3P model for water.[21,22] At the interface between the QM and MM region, hydrogen "link atoms" are used to satisfy the valency of the QM fragments. In the original implementation of the link-atom approach,[17c] electrostatic interactions between the link atom and the rest of the protein atoms were not included in the quantum calculation. This, however, introduces an imbalance in electrostatic interactions in the QM region due to the fact that molecular orbitals are delocalized, resulting in unrealistically large partial charges (ca. 0.3 e units) on link atoms. To correct this artifact, all electron integral terms are included in the formation of the Fock matrix in the present computation.

To corroborate the semiempirical method for the present thiophosphate formation reaction, crystal structures of similar thiophosphate ester compounds and ab initio MP2/6-31+G* energetic results for model reactions are employed to compare with that obtained from semiempirical calculations. It was found that the mixture of MNDO parameters for sulfur and phosphorus, and AM1 parameters for other atoms yields the best agreement (Table 1). In particular, the S−P bond distance is predicted to be 2.176 Å in methanethiophosphate ester using the AM1/MNDO model, which is in reasonable agreement with the crystal structural result (2.116 Å) for 2-(3-aminopropyl)-aminoethanethiophosphate, and other S−P bond distances (2.05−2.10 Å).[23] For comparison, the AM1 and HF/6-31+G* optimizations give S−P distances of 2.473 and 2.407 Å for methanethiophosphate dianion.[20,24]

The computed enthalpy changes for the model reactions, $CH_3S^- + CH_3OPO_3^{2-} \rightarrow CH_3O^- + CH_3SPO_3^{2-}$, and $H_2O + CH_3SPO_3^{2-} \rightarrow CH_3SH + HOPO_3^{2-}$, are 17.2 and 1.2 kcal/mol, respectively, using

(11) (a) Lim, C.; Karplus, M. *J. Am. Chem. Soc.* **1990**, *112*, 5872. (b) Dejaegere, A.; Lim, C.; Karplus, M. *J. Am. Chem. Soc.* **1991**, *113*, 4353. (c) Gorenstein, D. A.; Luxon, B. A.; Findley, T. B. *J. Am. Chem. Soc.* **1979**, *101*, 5869.

(12) (a) Schweins, T.; Warshel, A. *Biochemistry* **1996**, *35*, 14232. (b) Fothergill, M.; Goodman, M. F.; Petruska, J.; Warshel, A. *J. Am. Chem. Soc.* **1995**, *117*, 11619. (c) Florian, J.; Warshel, A. *J. Am. Chem. Soc.* **1997**, *119*, 15473. (d) Schweins, T.; Warshel, A. *Nat. Struct. Biol.* **1995**, *2*, 36.

(13) (a) Wo, Y.-Y. P.; Zhou, M.-M.; Stevis, P.; Davis, J. P.; Zhang, Z.-Y.; Van Etten, R. L. *Biochemistry* **1992**, *31*, 1712. (b) Pot, D. A.; Woodford, T. A.; Remboutsika, E.; Haun, R. S.; Dixon, J. E. *J. Biol. Chem.* **1991**, *266*, 19688.

(14) (a) Walsh, E. O. *Nature* **1952**, *169*, 546. (b) Herr, E. B., Jr.; Koshland, D. E., Jr. *Biochim. Biophys. Acta* **1957**, *25*, 219. (c) Bruice, T. C.; Benkovic, S. J. In *Bioorganic Mechanisms*; Benjamin, W. A.: New York, 1966; Vol. II, pp 1−103.

(15) Hansson, T.; Nordlund, P.; Aqvist, J. *J. Mol. Biol.* **1997**, *265*, 118.

(16) (a) Gao, J. *Acc. Chem. Res.* **1996**, *29*, 298. (b) Gao, J. In *Reviews in Computational Chemistry*; Lipkowitz, K. B., Boyd, D. B., Eds.; VCH: New York, 1995; Vol. 7, pp 119−185.

(17) (a) Warshel, A.; Levitt, M. *J. Mol. Biol.* **1976**, *103*, 227. (b) Singh, U. C.; Kollman, P. A. *J. Comput. Chem.* **1986**, *7*, 718. (c) Field, M. J.; Bash, P. A.; Karplus, M. *J. Comput. Chem.* **1990**, *11*, 700. (d) Tapia, O.; Colonna, F.; Angyan, J. G. *J. Chim. Phys.* **1990**, *87*, 875. (e) Gao, J. *J. Phys. Chem.* **1992**, *96*, 537. (f) Thompson, M. A.; Schenter, G. K. *J. Phys. Chem.* **1995**, *99*, 6374. (g) Gao, J. *J. Comput. Chem.* **1997**, *18*, 1061.

(18) (a) Liu, H.; Shi, Y. *J. Comput. Chem.* **1994**, *15*, 1311. (b) Hartsough, D. S.; Merz, K. M., Jr. *J. Phys. Chem.* **1995**, *99*, 384. (b) Lyne, P. D.; Mullholland, A. J.; Richards, W. G. *J. Am. Chem. Soc.* **1995**, *117*, 11345.

(19) (a) Gao, J.; Xia, X. *Science* **1992**, *258*, 631. (b) Gao, J.; Pavelites, J. J. P. *J. Am. Chem. Soc.* **1992**, *114*, 1912. (c) Gao, J.; Xia, X. *J. Am. Chem. Soc.* **1993**, *115*, 9667. (d) Sehgal, A.; Shao, L.; Gao, J. *J. Am. Chem. Soc.* **1995**, *117*, 11337. (e) Gao, J. *J. Am. Chem. Soc.* **1995**, *117*, 8600. (f) Gao, J.; Freindorf, M. *J. Phys. Chem. A* **1997**, *101*, 3182.

(20) (a) Dewar, M. J. S.; Zoebisch, E. G.; Healy, E. F.; Stewart, J. J. P. *J. Am. Chem. Soc.* **1985**, *107*, 3902. (b) Dewar, M. J. S.; Thiel, W. *J. Am. Chem. Soc.* **1977**, *99*, 4907.

(21) (a) MacKerell, A. D., Jr.; Karplus, M. *CHARMM-22 force field*. Harvard University, 1996. (b) Brooks, B. R.; Bruccoleri, R. E.; Olafson, B. D.; States, D. J.; Swaminathan, S.; Karplus, M. *J. Comput. Chem.* **1983**, *4*, 187. (c) Chatfield, D.; Brooks, B. R. Unpublished results.

(22) Jorgensen, W. L.; Chandrasekhar, J.; Madura, J. D.; Impey, R. W.; Klein, M. L. *J. Chem. Phys.* **1983**, *79*, 926.

(23) (a) Karle, J. M.; Karle, I. L. *Acta Crystallogr.* **1988**, *C44*, 135. (b) Kennard, O.; Allen, F. H.; Bellard, S.; Brice, M. D.; Cartwright, B. S.; Doubleday: A.; Higgs, H.; Hummelink, T.; Hummelink-Peters, B. G.; Motherwell, W. D. S.; Rodgers, J. R.; Watson, D. G. *Acta Crystallogr.* **1979**, *B35*, 2331.

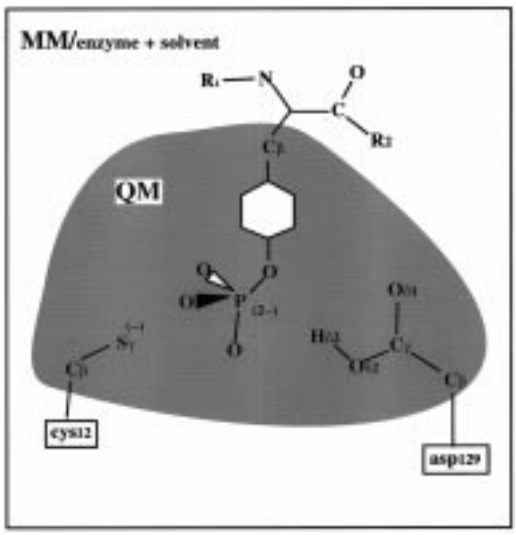

Figure 1. A schematic representation of the quantum mechanical and molecular mechanical partition in the molecular dynamics simulation of bovine protein tyrosine phosphatase.

Table 1. Computed energy of reactions for the model systems (kcal/mol)

$$CH_3OPO_3^{=} + CH_3S^- \rightarrow CH_3O^- + CH_3SPO_3^{=} \quad (1)$$

$$C_6H_5O^- + CH_3COOH \rightarrow C_6H_5OH + CH_3COO^- \quad (2)$$

$$CH_3SPO_3^{=} + H_2O \rightarrow CH_3SH + HOPO_3^{=} \quad (3)$$

reaction	exp	AM1/MNDO	HF/6-31+G*	MP2/6-31+G*
1	10.5[a]	17.2	30.1	16.0
2	−1.6	5.5	−2.6	−2.5
3	5.6	1.2	5.6	13.7

[a] Estimated on the basis of Benson's additivity rules for methanethiophosphate dianion. Experimental values are calculated from experimental heats of Formation.

the AM1/MNDO model. This may be compared with values of 30.1 and 5.6 kcal/mol obtained at the HF/6-31+G*//6-31+G* level, and 16.0 and 13.7 kcal/mol at the MP2/6-31+G* level. The proton-transfer reaction between acetic acid and phenoxide ion was also examined using the AM1 model, which yields an enthalpy of reaction of 5.5 kcal/mol. Experimental proton affinity data favors the proton transfer by −1.6 kcal/mol. The discrepancy is due to an underestimate of the heat of formation for acetate ion by the AM1 model (−116.0 kcal/mol) in comparison with experiment (−122.5) kcal/mol.[20] Although the use of mixed MNDO and AM1 parameters are not recommended for general applications, overall, the combination leads to reasonable results in the present application for this particular reaction. This may be viewed as a set of reaction specific semiempirical parameters for the thiophosphate reaction. Work is in progress to develop a more general set of reaction specific parameters for other phosphate hydrolysis reactions. In closing this section, we note that Warshel and co-workers have extensively used an empirical valence bond (EVB) approach to study enzymatic reactions including phosphate hydrolysis reactions.[25] In that case, the empirical parameters are calibrated to fit against experimental properties of model systems in solution.

B. Modeling. The X-ray crystal structure of BPTP determined by Zhang et al. is used as the starting point for molecular dynamics simulations.[6a] Initial coordinates of the enzyme−substrate complex are obtained by docking a tyrosine phosphate dianion residue into the active site region, with the position of the crystallographically determined phosphate ion as the anchoring point. BPTP has its maximum activity in the pH range of 4−8, according to which the state of all titratable residues is assigned.[8,26] Consequently, the two histidine residues (His66 and His72) are protonated in accord with experimental pK_a values of 8.36 and 9.19, respectively.[26a,b] There are two cysteine residues in the active site of BPTP, Cys12 and Cys17. The pK_a of these two residues have been determined by titration with iodoacetate and iodoacetamide to be <4 for Cys12 and 9.1 for Cys17.[26c] The exceptionally low pK_a of Cys12 may be compared with that of Cys403 in the *Yersinia* PTPase (4.67)[26d] and is consistent with a thiolate anion nucleophile in the substitution reaction. Therefore, Cys12 is modeled as a thiolate anion. The aspartic acid (Asp129) has been determined to have a pK_a of 5.3 by Evans et al.[26c] and is modeled as a protonated acid in accord with the pH dependence of k_{cat}/K_m for BPTP.

To mimic the aqueous solvent environment, the enzyme system is surrounded by a 24 Å sphere of water molecules with stochastic boundary conditions.[27] Water molecules that are within 2.5 Å of protein heavy atoms are removed. This resulted in a total of 5917 atoms in the simulation sphere (Figure 2). This initial structure is then equilibrated through stochastic boundary molecular dynamics (SBMD) simulations for at least 300 ps.[27,28] To model the chemical process, the side chains of the tyrosine phosphate substrate, the nucleophilic residue Cys-12, and the general acid residue Asp-129 are represented quantum-mechanically,[16] and hydrogen "link-atoms" are added to satisfy the valency at the divided QM/MM bonds as described above. This QM system is embedded in the rest of the classical enzyme−solvent system, with the QM/MM bonds constrained by the SHAKE algorithm (Figure 1). A nonbonded cutoff radius of 12 Å, based on geometrical centers of interaction groups, is used for both QM/MM and MM interactions. As in previous studies, electrostatically neutral MM groups that are directly bonded to the QM fragment are not included in the QM/MM interaction.[17c] The entire QM system is treated as a single group in the present study.

C. Umbrella Sampling. The principal goal of the QM/MM-SBMD simulations is to obtain the potential of mean force (pmf), $\Delta G(R_c)$, as a function of the reaction coordinate R_c, which is defined as $R_c = R(P-O) - R(P-S)$, where $R(P-O)$ and $R(P-S)$ are distances between the phosphorus and the ester oxygen, and the Cys12 sulfur atom. The pmf is determined using the umbrella sampling technique, which has been widely used in the calculation of reaction profiles in solution.[29]

In eq 2, $g(R_c)$ is the probability of occurrence of configurations as a function of the reaction coordinate R_c. Simulations are performed at different regions along R_c by a restraining or biasing potential in the energy function.

$$\Delta G(R_c) = -RT \ln g(R_c) \quad (2)$$

The biasing potential can be properly chosen to allow adequate overlap between adjacent windows of the simulation (Figure 3). The effect due to the biasing potential is then removed in statistical analyses to yield $g(R_c)$. The umbrella sampling technique is preferred for enzymatic reactions over free energy perturbation methods because it imposes fewer geometrical constraints during the dynamics simulation. The drawback of the method is that a biasing potential is needed to ensure an efficient sampling along the entire reaction coordinate. This has to be determined through trial and error, although it can be conveniently done during the equilibration stage of the simulation. In the present study, the biasing function is fitted to a cubic spline function as

(24) Frisch, M. J.; Trucks, G. W.; Schlegel, H. B.; Gill, P. M. W.; Johnson, B. G.; Wong, M. W.; Foresman, J. B.; Robb, M. A.; Head-Gordon, M.; Replogle, E. S.; Gomperts, R.; Andres, J. L.; Raghavachari, K.; Binkley, J. S.; Gonzalez, C.; Martin, R. L.; Fox, D. L.; Defrees, D. J.; Baker, J. Stewart, J. J. P.; Pople, J. A. *Gaussian 92/DFT*, Revision G3; Gaussian, Inc.: Pittsburgh, PA, 1993.

(25) Warshel, A. *Computer Modeling of Chemical Reactions in Enzymes and in Solutions*; John Wiley & Sons: New York, 1991.

(26) (a) Davis, J. P.; Zhou, M.-M.; Van Etten, R. L. *J. Biol. Chem.* **1994**, *269*, 8734. (b) Tishmack, P. A.; Bashford, D.; Harms, E.; Van Etten, R. L. *Biochemistry* **1997**, *36*, 11984. (c) Evans, B.; Tishmack, P. A.; Pokalsky, C.; Zhang, M.; Van Etten, R. L. *Biochemistry* **1996**, *35*, 13609. (d) Zhang, Z.-Y.; Dixon, J. E. *Biochemistry* **1993**, *32*, 9340.

(27) Brooks, C. L.; Karplus, M. *Biopolymers* **1985**, *24*, 843.

(28) Alhambra, C.; Gao, J. Unpublished results.

(29) Valleau, J. P.; Torrie, G. M. In *Statistical Mechanics Part A: Equilibrium Techniques*; Berne, B. J., Ed.; Plenum: New York, 1977; p 137. Kottalam, J.; Case, D. A. *J. Am. Chem. Soc.* **1988**, *110*, 7690.

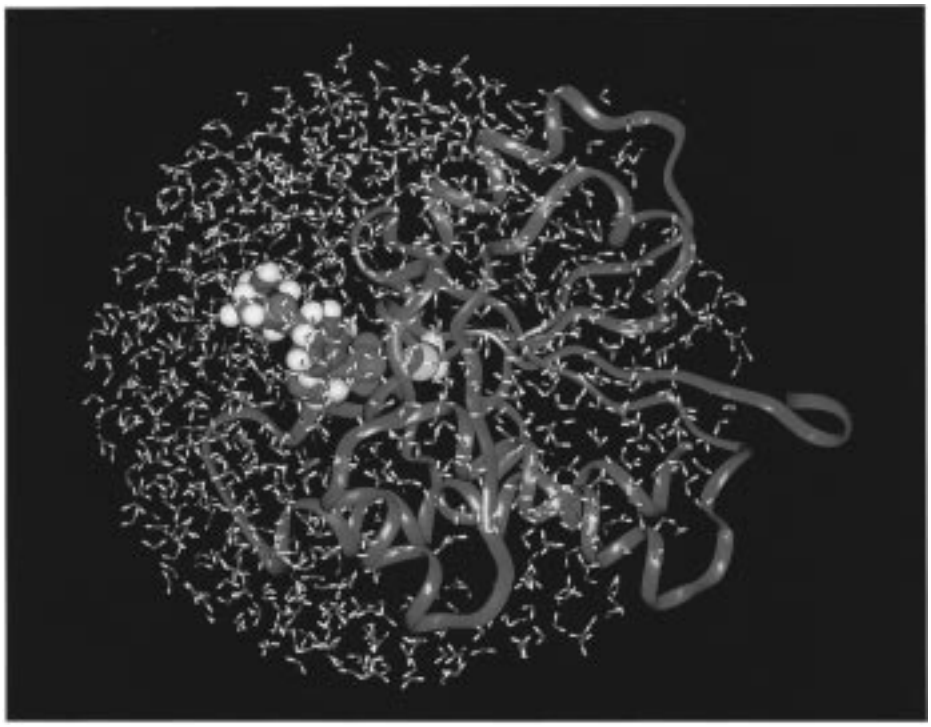

Figure 2. A schematic representation of the protein−solvent system used in the stochastic boundary molecular dynamics simulation. The center of the 24 Å is initially anchored at the location of the Cys12 sulfur atom. Protein backbones are illustrated by blue ribbons, while the quantum mechanically treated residues are indicated by the CPK model.

described previously.[30] The simulations were carried out in 10−12 overlapping regions to cover the entire reaction coordinate, each consisting of at least 25 ps for equilibration and 20 ps of averaging. The reaction coordinate R_c was constrained within a limited range by imposing a harmonic force, although the P−O and P−S bond distances are allowed to freely vary during the simulation. Thus, the associative or dissociative nature of the transition state is not affected by the computational constraints. The pmf was first determined for the reaction of tyrosine phosphate dianion in BPTP. To assess a recent mechanistic proposal that PTPases react with monoanionic phosphate in the active site,[15] the reaction profile was also determined for the monoanion substrate. All calculations were performed using a modified version of CHARMM at a temperature of 300 K.[21b,c]

D. Determination of Activation Parameters. The low molecular weight phosphatase from bovine heart (BPTP) was purified to homogeneity as described previously.[4b] *p*-Nitrophenyl phosphate (pNPP) was purchased from Sigma. Pre-steady-state kinetic measurements of the BPTP-catalyzed hydrolysis of pNPP were conducted using a Hi-Tech SF-61 stopped-flow spectrophotometer (dead time, 2 ms) with an observation cell length of 1.0 cm. Fast reactions were studied at pH 7 by monitoring the increase in absorbance at 410 nm of the *p*-nitrophenolate product.[8a] The buffer used was 50 mM 3,3-dimethylglutarate, 1 mM EDTA, I = 0.15 M adjusted by adding NaCl. The enzyme concentration ranged from 10 to 25 μM and the pNPP concentration varied from 20 to 50 mM. Data were collected on a Macintosh computer interfaced to the stepped-flow spectrophotometer using the program KISS (Kinetic Instruments, Inc.). Each stopped-flow trace was an average of at least 6 individual experiments. The specific rate constants were analyzed by fitting the experimental data directly to the theoretical equation through the use of the nonlinear square algorithm in KISS. The analysis of burst kinetics has been described previously.[31d] Briefly, when [S] ≫ [E], the increase in *p*-nitrophenolate concentration as a function of time can be described as [*p*-nitrophenolate] = $At + B(1 - \exp[-bt])$. When the experiments are performed at saturating concentrations of substrate, the individual rate constants for the enzyme phosphorylation (k_2) and dephosphorylation (k_3) can be determined from the experimental $b = k_2 + k_3$, and the linear phase $A = k_2k_3/(k_2 + k_3)$, respectively (Scheme 1). The size of the burst $B = E_0[k_2/(k_2 + k_3)]^2/(1 + K_m/S_0)^2$ is proportional to the active enzyme concentration. The temperature dependencies of rate constants from 4 to 23 °C are listed in Table 2 for each of the individual chemical steps. As observed previously,[8a] burst kinetics was obeyed at each temperature with the rate-limiting step being the hydrolysis of the intermediate (k_3), and the burst size corresponded to the stoichiometric concentration of BPTP. Activation parameters calculated from the data in Table 2 are the following: $\Delta H^{\ddagger} = 12.0$ kcal/mol and $\Delta S^{\ddagger} = -7.8$ cal/(mol) K) for k_2 step; $\Delta H^{\ddagger} = 13.7$ kcal/mol and $\Delta S^{\ddagger} = -8.6$ cal/(mol K) for k_3 step.

Results and Discussion

A. Reaction Profiles. The computed pmf for the first step in the dephosphorylation reaction of Cys12 thiolate with tyrosine phosphate dianion catalyzed by BPTP is shown in Figure 4, along with that for the reaction of the tyrosine phosphate monoanion substrate. The computed activation free energy $\Delta G^{\ddagger}$ for the first chemical step of the reaction, k_2 (Scheme 1), is 13.9 ± 0.5 kcal/mol for the dianion substrate and 15.7 ± 0.5 kcal/mol for the monoanion. Activation parameters for both phosphoenzyme formation (k_2) and hydrolysis (k_3) have been determined experimentally by analyzing the temperature dependencies for each step (Scheme 1). The free energy of activation for the initial phosphorylation reaction is 14.3 kcal/mol at 298 K. Typically, the rate-limiting step in PTPases-catalyzed reactions is the second, phosphoenzyme hydrolysis step, which has an activation free energy of 16.3 kcal/mol for BPTP. Thus, the predicted $\Delta G^{\ddagger}$ for the dianion substrate is in accord with experiment, indicating that the semiempirical method is reasonable for this particular system.

Interestingly, our computational results reveal that the reaction of the dianion substrate is preferred in the active site of BPTP

(30) Gao, J. *J. Am. Chem. Soc.* **1991**, *113*, 7796.

(31) (a) Hengge, A. C.; Sowa, G. A.; Wu, L.; Zhang, Z.-Y. *Biochemistry* **1995**, *34*, 13982. (b) Hengge, A. C.; Denu, J. M.; Dixon, J. E. *Biochemistry* **1996**, *35*, 7084. (c) Hengge, A. C.; Zhao, Y.; Wu, L.; Zhang, Z.-Y. *Biochemistry* **1997**, *36*, 7928. (d) Zhang, Z.-Y.; Zhou, G.; Denu, J. M.; Wu, L.; Tang, X.; Mondesert, O.; Russell, P.; Butch, E.; Guan, K.-L. *Biochemistry* **1995**, *34*, 10560.

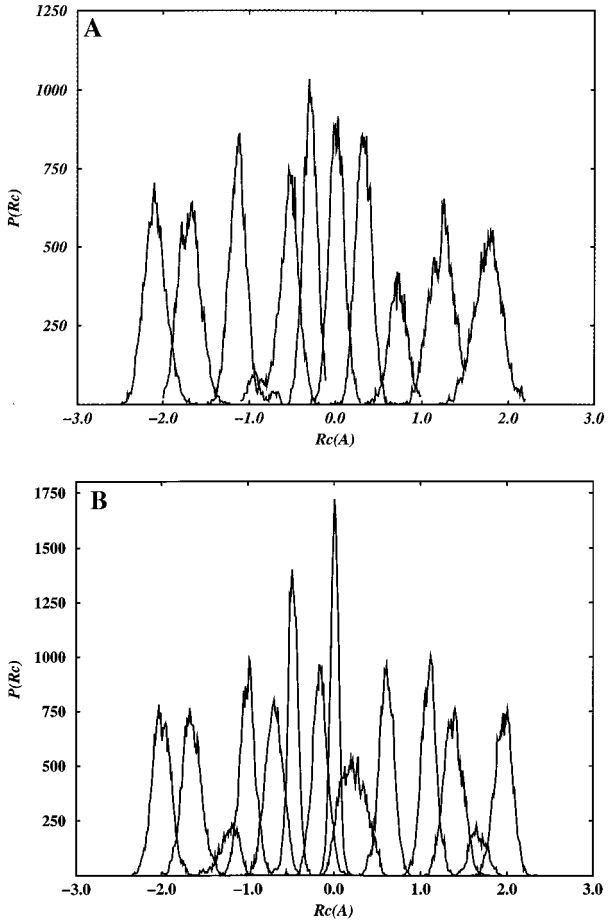

Figure 3. Structure distributions $P(R_c)$ along the reaction coordinate R_c from umbrella sampling simulations for the reaction of the phosphate dianion (a) and monoanion (b) in BPTP. $P(R_c)$ is converted to $g(R_c)$ by removing the biasing effect in statistical analyses. Units for the ordinate are given in number of configurations.

Scheme 1. The Kinetic Scheme for the BPTP-Catalyzed Reaction[a]

$$E + ArOPO_3^{2-} \underset{k_{-1}}{\overset{k_1}{\rightleftharpoons}} E\cdot ArOPO_3^{2-} \xrightarrow{k_2} E\text{-}P \xrightarrow{k_3} E + P$$

$$E\cdot ArOPO_3^{2-} \xrightarrow{k_2} ArOH$$

[a] The mechanism consists of substrate binding followed by two chemical steps, phosphorylation (k_2) and dephosphorylation (k_3). E is the enzyme, $ArOP_3^{2-}$ is the substrate, $E\cdot ArOP_3^{2-}$ is the enzyme−substrate Michaelis complex, E−P is the phosphoenzyme intermediate, ArOH is the phenol, and P_i is the phosphate ion.

Table 2. Temperature dependence of the rate coefficients for the phosphoenzyme formation (k_2) and the hydrolysis (k_3) reactions catalyzed by the low molecular weight bovine heart phosphatase against *p*-nitrophenyl phosphate

T (K)	k_2 (s^{-1})	k_3 (s^{-1})
277	40.0	1.10
283	67.3	1.91
288	91.0	3.31
296	177.0	5.70

over that of the protonated phosphate monoanion by 1.7 kcal/mol. Recently, Hansson et al. suggested that binding of the dianion to PTPases is disfavored because of electrostatic repulsion between the nucleophile thiolate anion (Cys12) and the substrate phosphate dianion.[15] Consequently, the reactive form of the substrate in the active site of PTPases is the monoanion, resulting either from a proton transfer from Cys12 to the phosphoryl dianion during the reaction or from binding

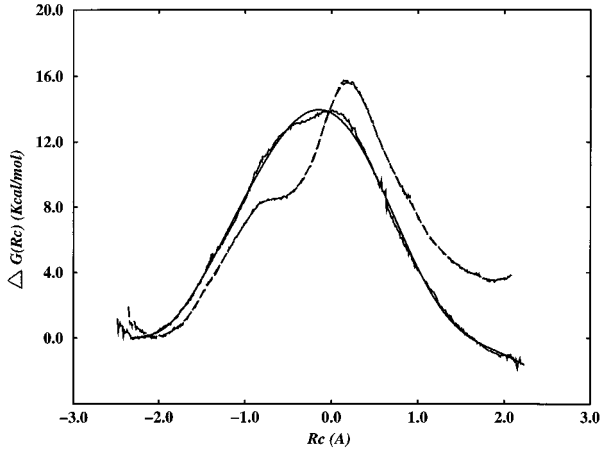

Figure 4. Calculated potential of mean force for the dianion (solid curve) and monoanion (dashed curve) system in BPTP as a function of the reaction coordinate, R_c (in angstroms). Smoothed curves are from a polynomial least-squares fit of the computed data.

of the phosphate monoanion if Cys12 existed as a thiolate anion.[15] However, experimental pH-rate profiles and pH-dependent inactivation data for all known PTPases show that the active form of the substrate is a dianion and that the nucleophilic Cys ($pK_a < 4.0$ in BPTP) is a thiolate ion at physiological pH.[3,26] Furthermore, the $^{18}(V/K)_{nonbridge}$ isotope effects for PTPases are inconsistent with the proposal involving a proton transfer from the active site Cys to the phosphoryl group.[31] Such protonation would result in large inverse effects, which are not observed.[31] Although the present study does not directly address the question of substrate binding, it indicates that there is no catalytic advantage for a monoanion substrate in BPTP.

The reaction of the dianion shows a unimodal energy profile, typical of an S_N2 reaction mechanism, with an average P−O and P−S distances of 2.15 ± 0.08 and 2.28 ± 0.07 Å in the transition state region ($R_c = -0.14$ Å). The average charge separation between the phosphoryl unit and the phenoxy leaving group at the transition state is estimated to be 0.89 e on the basis of Mulliken population analysis. This represents a gain of 0.28 e in charge density in comparison with the total charge of the phenoxy group in the ground state (−0.61 e). The charge development on the leaving group at the transition state is stabilized by the general acid residue Asp129 and a water molecule through hydrogen-bonding interactions.[2−4] The rather advanced charge separation between PO_3 and the leaving group suggests that kinetic isotope effects (KIE) for atoms of the leaving group would exhibit a dissociative-like transition state behavior, although the phenoxy oxygen is still in close contact with the phosphorus. This expectation is consistent with experimental heavy-atom isotope results for the bridging oxygen and the nitrogen of *p*-nitrophenol phosphate ester in PTPases.[31] On the other hand, the formation of the S−P bond is substantial in view of the bond distance at the transition state. The net charge of the Cys12 thiolate group decreases from −1.0 e in the ground state to −0.76 e in the transition state. Interestingly, the total charge on the PO_3 group remains virtually unchanged from the ground state (−1.36 e) to the transition state (−1.32 e), suggesting that the P−O bond order for the equatorial oxygens has minimal variation. In fact, there is slight decrease (0.04 e) in partial charge on the phosphoryl group at the transition state. Typically, the $^{18}(V/K)_{nonbridge}$ effects are found to be close to unity in PTPase-catalyzed reactions.[31]

A bimodal reaction profile is obtained for the monoanion, corresponding respectively to the breakage of a hydrogen bond

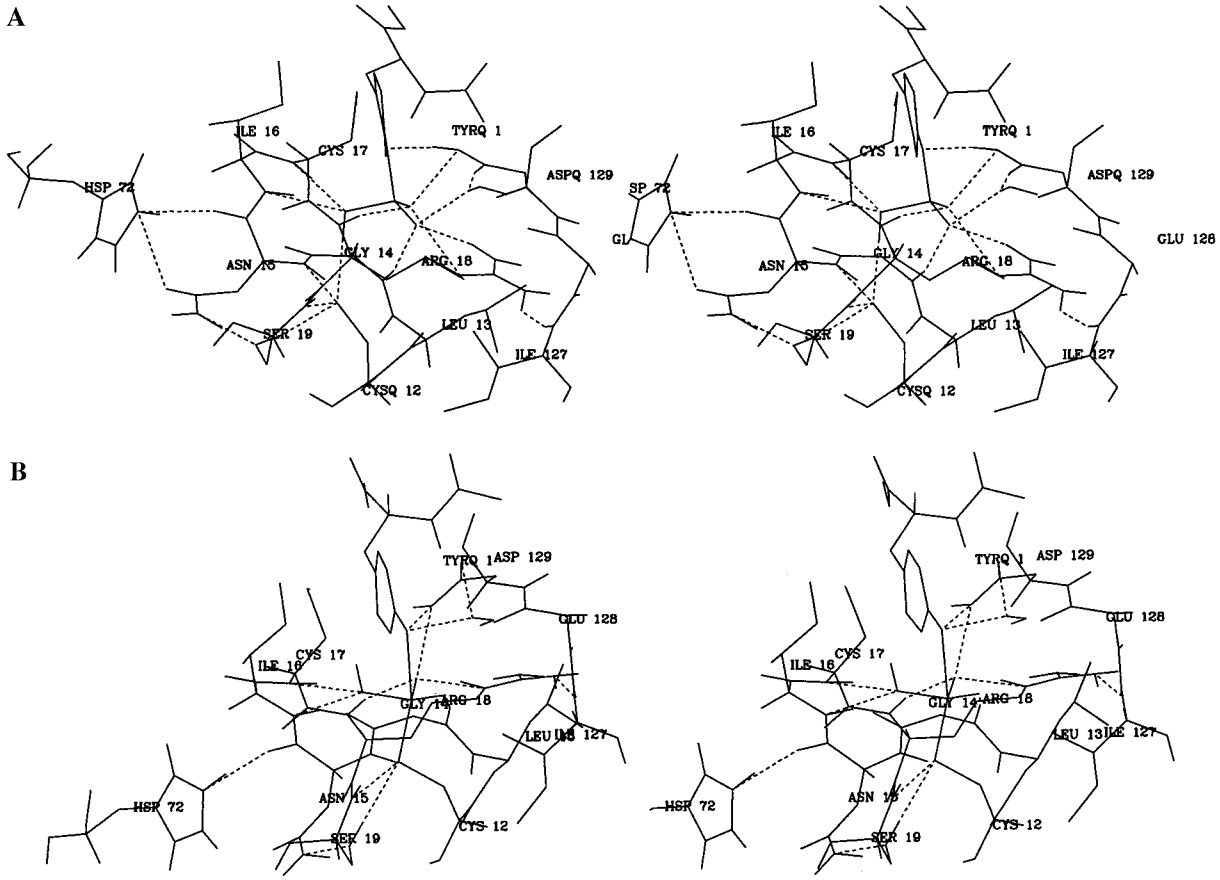

Figure 5. Hydrogen-bonding interactions for the ground state (a) and transition state (b) of phosphotyrosine monoanion in the active site of BPTP. The last structures from the hybrid QM/MM molecular dynamics simulations at $R_c = -2.0$ and 0.30 Å, respectively, are shown.

from the phosphate hydroxyl group to thiolate and the nucleophilic substitution step. The phosphate hydroxy group is initially oriented toward the Cys12 thiolate anion to form a hydrogen bond in the active site (Figure 5). As the thiolate anion approaches the phosphorus center, this hydrogen bond must be broken before the nucleophilic attack, and the phosphate hydroxy group is moved to the opposite direction of the nucleophile. This results in a higher overall activation barrier and a late transition state ($R_c = +0.18$ Å) for the tyrosine phosphate ester cleavage than the dianion.

B. Hydrogen-Bonding Patterns in the Michaelis Complex. The phosphate-binding site of protein tyrosine phosphatases is characterized by the signature sequence of $C(X)_5R(S/T)$ that is shared by all known PTPases including both high and low M_r enzymes.[3] The conserved residues Cys12 and Arg18 are essential for catalysis in BPTP, as do analogous residues in other PTPases.[3] This has been demonstrated by a complete loss of phosphatase activity when either amino acid is mutated to an alternative residue.[8c,32] In addition, correlation of biochemical results and the structure of BPTP revealed that Asp129 acts as a Brønsted acid catalyst in the first step of the phosphoryl transfer reaction[5,33] and that a number of other residues including Asn15, Ser19, and His72 can significantly affect the structure of the backbone of the phosphate-binding loop and the pK_a of Cys12.[26] Since both experimental and computational results support a dianion substrate in PTPases, the following discussion will focus on the reaction involving tyrosine phosphate dianion. Figure 6 illustrates hydrogen-bonding interactions in the active sites for the Michaelis complex and the transition structure, while hydrogen-bond distances are listed in Table 3. All hydrogen-bond distances are given between heavy atoms, which have been averaged over molecular dynamics trajectories in regions corresponding to the Michaelis complex ($R_c = -2.0 \pm 0.3$ Å) and the transition state ($R_c = -0.15 \pm 0.10$ Å).

The structure of the phosphate-binding loop is maintained by a series of hydrogen-bonding interactions involving the backbone carbonyl groups of the loop and the side chain of Arg18, radiating from the active-site cleft. The position of Arg18 is fixed by two hydrogen bonds: one between an N_{η^2} hydrogen and the backbone carbonyl oxygen of Ile127 (2.83 ± 0.14 Å), and another between the second N_{η^2} hydrogen and a water molecule which bridges with Asp92. These interactions are in accord with the X-ray structure of BPTP.[6a] His72 participates in hydrogen-bonding interactions with the side chain of Ser19 (2.82 ± 0.12 Å) and the carbonyl group of Asn15 (3.31 ± 0.20 Å), providing additional stabilization to the geometry of the phosphate-binding loop. Importantly, the interactions between His72 and the side chains of Asn15 and Ser19 enforce their hydrogen-bond donating ability, providing important contributions to the stabilization of the nucleophilic thiolate anion of Cys12. The structural function of His72 in BPTP is reflected by site-directed mutagenesis experiments. Removal of His72 in the H72A mutation decreases the catalytic activity to about 15% of that of the wild-type enzyme, while

(32) (a) Zhang, Z.-Y.; Wu, L. *Biochemistry* **1997**, *37*, 1362. (b) Cirri, P.; Chiarugi, P.; Camici, G.; Manao, G.; Raugei, G.; Cappugi, G.; Ramponi, G. *Eur. J. Biochemistry* **1993**, *214*, 647. (c) Zhang, Z.-Y.; Wang, Y.; Wu, L.; Fauman, E.; Stuckey, J. A.; Schubert, H. L.; Saper, M. A.; Dixon, J. E. *Biochem.* **1994**, *33*, 15266.

(33) Zhang, Z.; Harms, E.; Van Etten, R. L. *J. Biol. Chem.* **1994**, *249*, 25947. (b) Taddeo, N.; Chiarugi, P.; Cirri, P.; Fiaschi, T.; Stefani, M.; Camici, G.; Giovanni, R.; Ramponi, G. *FEBS Lett.* **1994**, *350*, 328. (c) Zhang, Z.-Y.; Wang. Y.; Dixon, J. E. *Proc. Natl. Acad. Sci. U.S.A.* **1994**, *91*, 1624.

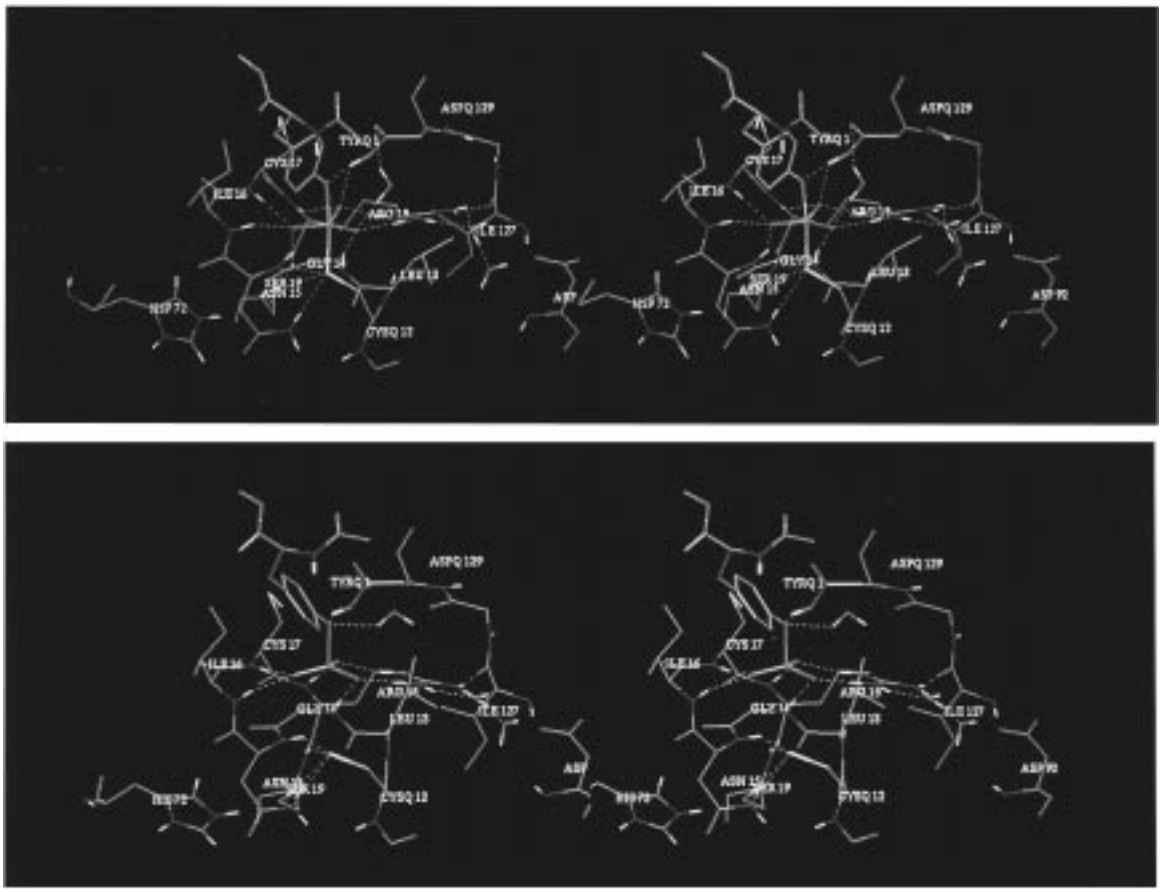

Figure 6. Hydrogen-bonding interactions for the ground state (a, bottom) and transition state (b, top) of phosphotyrosine dianion in the active site of BPTP. The last structures from the hybrid QM/MM molecular dynamics simulations at $R_c = -2.0$ and -0.30 Å, respectively, are shown.

an experimentally significant decrease in binding affinity has also been observed.[26c]

The substrate phosphotyrosine monoester is accommodated in the active site of BPTP with the phenoxy group surrounded by hydrophobic side chains. Because of steric hindrance, the Tyr residue is oriented toward the opposite side of the nucleophilic Cys12 and is partially exposed to the solvent. This enforces an in-line nucleophilic attack from the thiolate anion in the substitution reaction. The phosphate dianion is held in close proximity of the phosphate-binding loop through a series of hydrogen-bonding interactions with the backbone hydrogen atoms as well as with the side chain of Arg18. On average, each phosphate oxygen forms at least two strong hydrogen bonds and one relatively longer hydrogen bond (Table 3). As depicted in Figure 6a, the first phosphate oxygen (O_1) at the start of the phosphate-binding loop is hydrogen bonded to the backbone NH of Gly14 and the $N_\eta H$ of Arg18 with average distances of 2.93 and 2.87 Å, respectively. The third hydrogen bond with Leu13 is somewhat longer at a distance of 3.45 Å. This is followed by three main chain NH hydrogen bonds to the second phosphate oxygen (O_2) from Asn15 (2.98 Å), Ile16 (2.81 Å), and Cys17 (3.02 Å) in the central region of the loop, although the NH group of Asn15 is situated in a direction pointing to the S_γ of Cys12. The third oxygen is anchored by interactions with the main chain NH (2.98 Å) and the side chain $N_\epsilon H$ (2.85 Å) of Arg18. These hydrogen bonds are maintained along the entire reaction coordinate during the molecular dynamics simulations, although differences exist in hydrogen-bond distance at the transition state and ground state (see below). The bifurcated ion pair interaction between the phosphate dianion and Arg18 emphasizes the essential role of this residue for substrate binding. Mutation of Arg18 to any other residues completely deactivates phosphatase activity,[8c] although substitution by a Lys retains phosphate binding affinity.[32c]

Table 3. Selected average hydrogen bond distances between heavy atoms for the ground and transition state of phosphotyrosine dianion in the active site of bovine protein tyrosine phosphatase (Å)

H-bond acceptor	H-bond donor	Michaelis complex	transition state
O_a	Asp129 $O_{\delta 1}$	2.90 ± 0.13	2.89 ± 0.11
	Cys17 S_γ	4.10 ± 0.30	3.92 ± 0.23
	Wat702 O	3.39 ± 0.27	3.00 ± 0.15
O_1	Leu13 N	3.45 ± 0.22	2.90 ± 0.11
	Gly14 N	2.93 ± 0.11	3.00 ± 0.13
	Arg18 N_{η^1}	2.87 ± 0.11	3.05 ± 0.34
	Wat702 O	2.96 ± 0.22	2.86 ± 0.15
O_2	Asn15 N	2.98 ± 0.15	2.89 ± 0.20
	Ile16 N	2.81 ± 0.07	2.75 ± 0.08
	Cys17 N	3.02 ± 0.19	2.93 ± 0.13
O_3	Arg18 N	2.98 ± 0.13	2.91 ± 0.18
	Arg18 N_ϵ	2.85 ± 0.09	2.81 ± 0.08
	Arg18 N_{η^1}	3.64 ± 0.15	3.44 ± 0.19
Ile127 O	Arg18 N_{η^2}	2.83 ± 0.14	2.95 ± 0.16
Cys12 S	Asn15 N	3.73 ± 0.18	3.67 ± 0.17
	Asn15 N_δ	3.23 ± 0.11	3.40 ± 0.15
	Ser19 N	3.64 ± 0.20	3.66 ± 0.17
	Ser19 O_γ	3.03 ± 0.09	3.14 ± 0.11

Both Cys17 and Asp129 form hydrogen bonds to the bridging ester oxygen of the substrate at distances of 4.10 ± 0.30 and 2.90 ± 0.13 Å, respectively. The specific role of Cys17 is still uncertain experimentally.[8c] The weak hydrogen-bonding interactions observed in the present study indicate that they may

provide some electrostatic stabilization to the leaving group. Asp129 has been proposed to donate a proton to the bridging ester oxygen during the substitution reaction. For example, mutation of similar aspartic acids that have been identified as the general acid residue in a number of PTPases, including the dual-specificity phosphatase VHR, the low M_r PTPase Stp1, and the *Yersinia* PTPase, typically reduces their activity against *p*-nitrophenyl phosphate by 2 to 3 orders of magnitude.[33] This translates to about 2 to 4 kcal/mol in activation free energy. In the present study, proton transfer from Asp129 to the phenoxide ion did not take place because the heat of formation for acetate ion is underestimated by the AM1 model (Table 1). However, strong hydrogen-bonding interactions are present during the reaction. In view of the kinetic data for the mutant enzymes, the computed activation barrier may be overestimated by about 1−2 kcal/mol due to a lack of proton transfer during the reaction.

Two major factors contribute to the activity of the nucleophile Cys12 in the substitution reaction of phosphotyrosine monoester: (1) the protonation state of Cys12 and (2) the position of the nucleophile in the active site. Figure 6a reveals that, in addition to the phosphate-binding region, the active site of BPTP also contains a thiolate anion stabilizing region. Experimentally, the pK_a of the nucleophilic Cys is <4 in BPTP and 4.7 in the *Yersinia* PTP, and experimental evidence for all PTPases indicates that the nucleophilic cysteine is ionized prior phosphate binding.[3] Classical molecular dynamics simulations of the free enzyme in water indicate that an anionic Cys helps to stabilize the phosphate-binding loop by neutralizing the positive charge of Arg18 and hydrogen-bonding interactions with the backbone amide hydrogens.[28] As shown in Figure 6a, in the Michaelis complex, the S_γ atom are hydrogen bonded to the side-chain amide hydrogen of Asn15 (3.23 Å), the hydroxy group of Ser19 (3.03 Å), and the backbone amide hydrogens of Asn15 (3.73 Å) and Ser19 (3.64 Å). These specific hydrogen-bonding interactions help to significantly stabilize the thiolate anion of Cys12 in the active site. These findings are in accord with the conclusion of Hansson et al. in that the protein environment stabilizes the thiolate anion.[15] In addition, the position of the Cys12 sulfur atom is secured by these interactions. While the tyrosine phosphate is positioned above the phosphate-binding loop, the sulfur atom of Cys12 is located at the center below the loop, making it possible, and well-suited for an "in-line", anionic nucleophilic attack (Figure 6a). The phosphate-binding loop provides an effective dielectric shield through hydrogen bonding and ion pair interactions with both the nucleophile and the substrate, screening electrostatic repulsions between the phosphate dianion and the nucleophilic thiolate monoanion. In aqueous solution, nucleophilic attack by an anionic nucleophile is not possible because of electrostatic repulsions, which necessarily enforce the anionic site of the nucleophile to orient in the opposite direction of the phosphorus atom in the anionic phosphate monoester or diester.

On the experimental side, both Asn15 and Ser19 are found to be critical to the catalytic efficiency of BPTP.[26c,33] Mutation of Asn15 or Ser19 to an alanine in BPTP retains about 0.33% of the activity of the wild-type enzyme.[26c] Thus, each mutation destroys a hydrogen bond to Cys12 such that the thiolate anion is no longer effectively stabilized and its structure is shifted away from the optimal position for the nucleophilic attack.

In the Michaelis complex, a water molecule was found to form a hydrogen bond with the ester oxygen at a distance of 3.39 Å (Figure 6a). In turn, this water is hydrogen bonded to two other waters immersing into the bulk. The position of this water molecule is the result of molecular dynamics simulations,

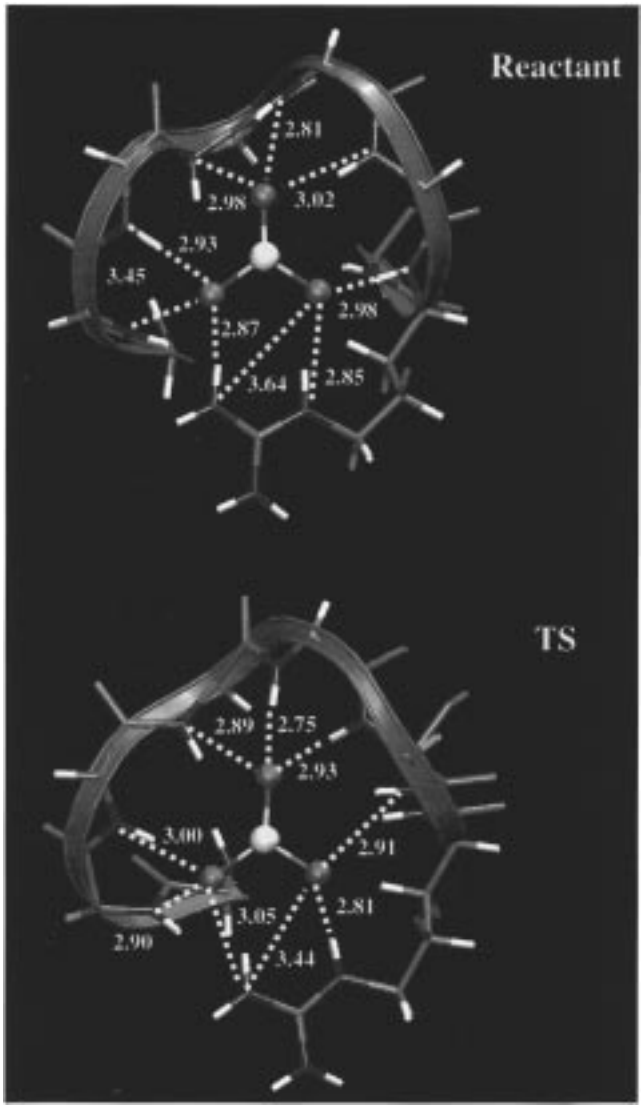

Figure 7. Hydrogen-bonding patterns for the phosphotyrosine dianion at the transition state and the enzyme−substrate complex in BPTP. Average hydrogen- bond distances for structures in regions of $R_c = -0.15 \pm 0.10$ Å (transition state, top) and $R_c = -2.0 \pm 0.3$ Å (ground state, bottom) are given in angstroms. For clarity, only the relevant phosphate group and backbone atoms in the phosphate-binding loop are shown. The view is made by looking down from Figure 6.

since crystallographilic water was not available in the BPTP structure. The active site is near the surface of the enzyme (Figure 2) and is partially exposed to the solvent. The position of this water molecule is subsequently shifted also to bridge hydrogen bonds between Asp129 and the phosphoryl O_1 oxygen in the transition state. Recently, a water molecule has been identified in the binding site from the X-ray crystal structures of the *Yersinia* PTPase complexed with tungstate and nitrate.[7b] A water molecule has also been found in the vicinity of the general acid Asp181 in the human PTP1B−substrate complex.[6c]

For phosphotyrosine ester monoanion, the thiolate anion of Cys12 forms a hydrogen bond with the hydroxy group of the phosphate (Figure 5), shifting the thiolate ion away from the optimal position for nucleophilic attack. Surprisingly, hydrogen-bonding patterns between the phosphate and the binding loop are remarkably similar to that of the dianion. The presence of a proton, nevertheless, shall significantly weaken the strength of these hydrogen bonds. It was suggested that a protonated phosphate monoanion is bound to PTPases because there would

Table 4. Comparison of ground and transition state hydrogen bond distances for the phosphorylation reaction with those of X-ray crystal structures of ligand-protein complexes in BPTP. Distances are given in angstroms

	computed		X-ray crystal structure[34]		
H-bond	reactant	TS	PO_4	MoO_4	VO_4
O_1−N Leu13	3.45	2.90	3.24	3.04	3.10
O_1−N Gly14	2.93	3.00	2.88	2.95	2.83
O_1−N_η Arg18	2.87	3.05	2.92	2.87	3.26
O_1−O wat	(2.96)	2.86			
O_2−N Asn15	2.98	2.89	3.36	3.18	3.24
O_2−N Ile16	2.81	2.75	2.87	2.69	2.55
O_2−N Cys17	3.02	2.93	2.73	2.71	2.48
O_3−N Arg18	2.98	2.91	3.30	3.09	2.80
O_3−N_ϵ Arg18	2.85	2.81	2.79	2.89	2.76
O_3−N_η Arg18	3.64	3.44	3.40	3.71	3.38

be a large energy penalty for bringing a doubly negatively charged phosphate and a singly charged anion together.[15] However, the negative charge of the thiolate anion is neutralized by the positive charge of Arg18, and its electric field would be positive in the phosphate-binding side and negative in the interior of the protein. This along with the surface arginine residues in close proximity at the binding site (Arg53 and Arg58) would provide a favorable electrostatic steering for binding of a dianionic substrate. In fact, experimental evidence of all PTPases studied to date supports the binding and reaction involving a phosphate dianion substrate.[3]

C. Differential Hydrogen-Bonding Interactions between the Ground and Transition State. Of particular interest are factors that contribute to enzyme catalysis and transition-state stabilization, in addition to the enzymatic activation and effective positioning of the Cys12 nucleophile. Figure 7 depicts hydrogen-bonding patterns between the phosphate group and the phosphate-binding loop for the enzyme−substrate complex (reactant) and the transition state in BPTP, along with average hydrogen-bond distances. There are marked changes in the hydrogen-bonding pattern between the transition state and the ground state due to structural reorganizations. The distance between the backbone nitrogen of Leu13 and the phosphoryl O_1 is reduced from 3.45 Å in the ground state to 2.90 Å in the transition state, which is accompanied by the formation of another hydrogen bond between phosphoryl O_1 and the active-site water molecule. The backbone amide group of Asn15 is reoriented from hydrogen bonding with the Cys12 sulfur to the direction of the phosphoryl O_2 atom. Concomitantly, the side chain of Arg18 is slightly shifted toward the O_3 atom. In addition, it is interesting to notice that hydrogen-bond distances are generally shortened by 0.05 to 0.1 Å on going from the reactant to the transition state for the dianion substrate. This is in good accord with recent X-ray diffraction studies by Zhang et al., who found an average reduction of 0.12−0.18 Å in hydrogen-bond distance when the equatorial oxygens in the vanadate inhibitor, which has a trigonal bipyramid geometry analogous to the transition state, are compared with either sulfonate or phosphate complex in BPTP (Table 4).[34] This structural variation would lead to enhanced hydrogen-bonding interactions between the thiolate−phosphate complex and the phosphate-binding loop.

Indeed, Zhang et al. pointed out on the basis of the crystallographic information that the transition state is differentially stabilized by hydrogen bonding relative to the ground and product states.[34] From hybrid QM/MM calculations for structures generated in the region of $R_c = -0.15 \pm 0.1$ Å, the transition state is estimated to be stabilized by the phosphate-binding loop relative to the reactant state at $R_c = -2.0$ Å by −4.6 to −6.2 kcal/mol, with and without internal energy contributions. Consistent with the conclusion of Zhang et al.,[34] the present study indicates that the Walden inversion in the S_N2 reaction enforces stronger hydrogen-bonding interactions at the transition state. This is accomplished through spatial expansion of the three oxygen atoms on going from the tetrahedral reactant to a trigonal bipyramidal geometry at the transition state, which pushes the oxygen atoms closer to the backbone amide groups and Arg18 side chain. Such a mechanical process may be used in the subsequent hydrolysis step of the phosphoenzyme intermediate in BPTP and is likely to be adopted by other PTPases, which all possess the same phosphate-binding loop.[3]

Conclusions

The present study explores the special structural features in the active site of the bovine low molecular weight protein tyrosine phosphatase using a combined QM/MM simulation model. It is found that the transition-state structure for the initial step of the phosphoryl transfer reactions is preferentially stabilized over the ground state through a Walden-inversion-enforced hydrogen-bonding mechanism in the active site. This is due to structural expansion of the phosphoryl oxygens on going from a tetrahedral geometry to the trigonal bipyramidal transition state in the S_N2 process and is supported by the development of shorter hydrogen bonds between the phosphate-binding loop and the phosphoryl oxygen atoms at the transition state. The present computational results are in accord with recent X-ray crystal structure data by Van Etten and co-workers for the transition-state analogue vanadate−BPTP complex in comparison with tetrahedral ions such as phosphate and sulfate. Furthermore, the present study suggest that a dianionic substrate is preferred in the BPTP-catalyzed phosphorylation reaction over the protonated monoanion because the latter process involves the breakage of a hydrogen bond between the nucleophile and the phosphoryl hydroxy group, which raises the overall barrier height.

Analyses of hydrogen-bonding patterns revealed that the active site contains both a phosphate-binding region and a thiolate anion stabilization region in the Michaelis complex. The latter interactions stabilizes the anionic nucleophilic residue Cys12 and positions the sulfur atom near the center below the phosphate-binding loop for an in-line nucleophilic attack. This is in contrast to reactions in solution where the more nucleophilic anions cannot be adequately aligned with the substrate for nucleophilic attack because of electrostatic repulsion. In the enzyme active site, the phosphate-binding loop provides an effective dielectric screening effect through hydrogen-bonding and ion pair interactions, making it possible for an anionic nucleophile to attack a dianionic substrate.

Acknowledgment. Gratitude is expressed to the National Institutes of Health (GM46736 and CA69202) for support of this research.

JA972578N

(34) Zhang, M.; Zhou. M.; Van Etten, R. L.; Stauffacher, C. V. *Biochemistry* **1997**, *36*, 15.